Available online at www.sciencedirect.com

ScienceDirect

Advances in Space Research 61 (2018) 2057–2073

ADVANCES IN SPACE RESEARCH (a COSPAR publication)

www.elsevier.com/locate/asr

Model based Computerized Ionospheric Tomography in space and time

Hakan Tuna [a,*], Orhan Arikan [a], Feza Arikan [b]

[a] Dept. of Electrical and Electronics Engineering, Bilkent University, Turkey
[b] Dept. of Electrical and Electronics Engineering, Hacettepe University, Turkey

Received 1 August 2017; received in revised form 21 January 2018; accepted 22 January 2018
Available online 2 February 2018

Abstract

Reconstruction of the ionospheric electron density distribution in space and time not only provide basis for better understanding the physical nature of the ionosphere, but also provide improvements in various applications including HF communication. Recently developed IONOLAB-CIT technique provides physically admissible 3D model of the ionosphere by using both Slant Total Electron Content (STEC) measurements obtained from a GPS satellite - receiver network and IRI-Plas model. IONOLAB-CIT technique optimizes IRI-Plas model parameters in the region of interest such that the synthetic STEC computations obtained from the IRI-Plas model are in accordance with the actual STEC measurements. In this work, the IONOLAB-CIT technique is extended to provide reconstructions both in space and time. This extension exploits the temporal continuity of the ionosphere to provide more reliable reconstructions with a reduced computational load. The proposed 4D-IONOLAB-CIT technique is validated on real measurement data obtained from TNPGN-Active GPS receiver network in Turkey.

Keywords: Ionospheric tomography; IRI-Plas model; GPS-STEC measurements; Kalman smoothing

1. Introduction

The electron density distribution in the ionosphere has a spatially and temporally varying structure. Due to the global nature of the main processes governing the ionization processes, electron density distribution in the ionosphere is highly correlated in space and time. For mid-latitude ionosphere, it has been observed that the temporal correlation or wide sense stationarity period can vary from 15 to 20 min for quiet days of the ionosphere, and from 3 to 25 min for disturbed days of the ionosphere (Sayin et al., 2010). To provide more robust results, the model based reconstructions of the electron density distribution from available set of measurements should exploit the temporal continuity in the physical structure of the ionosphere (Bilitza et al., 2014).

Classical approaches proposed for imaging the ionospheric electron density distribution use TEC measurements obtained between a Low Earth Orbit (LEO) satellite and an array of receiver stations, and take advantage of the smooth time-varying structure of the ionosphere. Measurements obtained at multiple time instants during a satellite pass are used for imaging a vertical slice of the electron density distribution. Since there is a significant time difference between the measurements, these methods assume ionosphere to be invariant during the duration of a satellite pass (Austen et al., 1988; Raymund et al., 1990; Pryse and Kersley, 1992; Andreeva et al., 1990; Foster et al., 1994).

GPS-STEC measurements obtained from all possible pairs of multiple satellites and receiver stations can give a snapshot of the ionosphere. CIT techniques utilizing GPS-STEC measurements in the literature are generally

* Corresponding author.
E-mail addresses: htuna@bilkent.edu.tr (H. Tuna), oarikan@ee.bilkent.edu.tr (O. Arikan), arikan@hacettepe.edu.tr (F. Arikan).

https://doi.org/10.1016/j.asr.2018.01.031
0273-1177/

described at a fixed time, and they handle the problem independently for each time instant resulting in limited performance (Ma et al., 2005; Arikan et al., 2007; Wen et al., 2008; Erturk et al., 2009; Tuna et al., 2015; Jin and Park, 2007). However, the ionosphere is highly correlated in time and GPS-STEC measurements have significant information about the past and future states of the ionosphere. In order to accommodate the temporal changes in the ionosphere, Kalman filtering is used in various approaches (Rius et al., 1997; Howe et al., 1998; Scherliess et al., 2004; Wang et al., 2004; Bust et al., 2004). Electron density values in reconstructed voxels are tracked in time by using Kalman filtering in Rius et al. (1997). The coefficients of the empirical orthogonal functions (EOFs) forming the perturbation values onto the default electron density values obtained from ionosphere models are tracked by using Kalman filtering in Howe et al. (1998). Kalman filtering is used in data assimilation approaches by linearization of physical models describing ionospheric parameters (Scherliess et al., 2004; Wang et al., 2004). Some methods using iterative approaches for 3D imaging of the ionosphere used previous reconstructions of the ionosphere as an initial estimate for the next time update by using Kalman filtering (Bust et al., 2004). A time-dependent algorithm for ionospheric imaging has also been proposed without using Kalman filtering techniques where electron density values are allowed to change linearly over time (Mitchell and Spencer, 2003). An iterative optimization method is used for finding the most smooth solution to the tomography problem in 4 dimensions in Nesterov and Kunitsyn (2011). The Fourier transform is also applied for forecasting global maps in Gulyaeva et al. (2013).

In this work, the IONOLAB-CIT technique, proposed in Tuna et al. (2015) for 3D imaging of the ionospheric electron density distribution, is extended to exploit the temporal structure of the ionosphere to provide more reliable reconstructions over time. Instead of tracking the ionospheric electron density distribution directly, reconstruction parameters of the IONOLAB-CIT, defining the perturbation surfaces on the spatial f_0F_2 and h_mF_2 surfaces, are tracked and smoothed in time by using Kalman filtering techniques. First, in order to investigate the temporal correlation among the IONOLAB-CIT results, the IONOLAB-CIT technique is applied on two sets of quiet and stormy days, providing reconstructions at every 15 min for the whole day. As expected, results of the experiments have indicated high temporal correlation that can be exploited by Kalman filtering techniques with improved performance. Second, possible state transition models for the IONOLAB-CIT results are proposed for estimating the temporal relation between consecutive states of the ionosphere and the temporal validity of these estimations are examined for increasingly longer time intervals. Finally, Kalman techniques are implemented for filtering/smoothing the IONOLAB-CIT results in time domain, for both obtaining more robust solutions and decreasing the computational cost of the IONOLAB-CIT technique. Results showed that Kalman filtering/smoothing techniques produce more robust reconstructions especially when the data from few GPS receivers are used in the reconstructions. The 4D-IONOLAB-CIT technique is presented in detail progressively in the following sections.

2. Regional CIT using the IRI-Plas model and the GPS-STEC measurements: IONOLAB-CIT

The IONOLAB-CIT technique is proposed in Tuna et al. (2015) for obtaining a robust 3D model of the electron density distribution in the ionosphere for a given time of the day. Since the proposed 4D-IONOLAB-CIT technique is based on an updated version of the IONOLAB-CIT technique, it is briefly reviewed below for the sake of completeness.

IRI-Plas is a parametric physical/empirical model which can estimate the monthly medians of the vertical electron density profile in the ionosphere and plasmasphere (Gulyaeva and Bilitza, 2012). However, IRI-Plas model generally does not produce compliant results with the real GPS-STEC measurements, which are widely used in ionospheric studies. The IONOLAB-CIT handles the CIT problem as an optimization problem where the objective is to find the optimum input parameters for the IRI-Plas model in the region of interest, such that the 3D electron density profile obtained from the IRI-Plas model complies with the available GPS-STEC measurements collected about the time of reconstruction. The input parameters of the IRI-Plas model that will be optimized are selected as the critical frequency of the F2 layer (f_0F_2) and the maximum ionization height (h_mF_2), which have significant effects on the electron density distribution in the ionosphere. However, rather than changing the f_0F_2 and the h_mF_2 parameters directly, IONOLAB-CIT technique tries to find the optimum parametric perturbation surfaces onto the default values of the f_0F_2 and the h_mF_2 surfaces that are provided by the IRI-Plas model.

The region of reconstruction in the IONOLAB-CIT technique is defined as:

$$A = \{(\phi, \lambda) | \phi_{min} \leqslant \phi \leqslant \phi_{max}, \lambda_{min} \leqslant \lambda \leqslant \lambda_{max}\}, \tag{1}$$

where ϕ and λ represents the latitude and the longitude, respectively. The following normalized coordinates bounded within $[-1\ 1]$ interval are used in the optimization problem for obtaining geometry free computations:

$$\phi_n = \frac{2\phi - \phi_{max} - \phi_{min}}{\phi_{max} - \phi_{min}}, \tag{2}$$

$$\lambda_n = \frac{2\lambda - \lambda_{max} - \lambda_{min}}{\lambda_{max} - \lambda_{min}}. \tag{3}$$

The first order parametric perturbation surfaces on the f_0F_2 and h_mF_2 surfaces provided by the IRI-Plas model in region A will be denoted by E_F and E_H, respectively. The following vector $\mathbf{m}$ holds the perturbation surface parameters for the f_0F_2 and h_mF_2 surfaces:

$$\mathbf{m} = \begin{bmatrix} \mathbf{m}^f \\ \mathbf{m}^h \end{bmatrix}, \tag{4}$$

where $\mathbf{m}^f = \begin{bmatrix} m_1^f & m_2^f & m_3^f \end{bmatrix}^T$ and $\mathbf{m}^h = \begin{bmatrix} m_1^h & m_2^h & m_3^h \end{bmatrix}^T$. Using these perturbation surface parameters, the first order perturbation surfaces E_F and E_H at any location in A can be expressed as:

$$E_F(\phi, \lambda, \mathbf{m}^f) = m_1^f \phi_n + m_2^f \lambda_n + m_3^f, \tag{5}$$

$$E_H(\phi, \lambda, \mathbf{m}^h) = m_1^h \phi_n + m_2^h \lambda_n + m_3^h. \tag{6}$$

Using E_F and E_H, perturbed f_0F_2 and h_mF_2 surfaces at any location in A can be expressed as:

$$F_p(\phi, \lambda, t, \mathbf{m}^f) = S\big(F(\phi, \lambda, t) + E_F(\phi, \lambda, \mathbf{m}^f), F_{min}, F_{max}\big), \tag{7}$$

$$H_p(\phi, \lambda, t, F_p(\phi, \lambda, t, \mathbf{m}^f), \mathbf{m}^h) = S\big(H(\phi, \lambda, t, F_p(\phi, \lambda, t, \mathbf{m}^f)) + E_H(\phi, \lambda, \mathbf{m}^h), H_{min}, H_{max}\big), \tag{8}$$

where $F(\phi, \lambda, t)$ is the f_0F_2 obtained from the IRI-Plas for the given latitude ϕ, the longitude λ and the time t, $F_p(\phi, \lambda, t, \mathbf{m}^f)$ is the perturbed f_0F_2 surface, $H(\phi, \lambda, t, F_p(\phi, \lambda, t, \mathbf{m}^f))$ is the h_mF_2 obtained from the IRI-Plas for the given latitude ϕ, the longitude λ, the time t, and the perturbed f_0F_2 parameter, $H_p(\phi, \lambda, t, F_p(\phi, \lambda, t, \mathbf{m}^f), \mathbf{m}^h)$ is the perturbed h_mF_2 surface, and finally S is a sigmoid-like function for bounding the perturbed parameters within given physical limits, $[F_{min} \quad F_{max}]$ and $[H_{min} \quad H_{max}]$.

Since, for any choice of $\mathbf{m}$ IRI-Plas model produces a physically admissible 3D electron density distribution, if $\mathbf{m}$ is chosen to minimize the difference between the real STEC measurements and the synthetic STEC values obtained from the reconstructed 3D electron density distribution, we obtain physically admissible reconstructions that comply with the measurements. The following cost function is defined for finding the optimum $\mathbf{m}$:

$$C(\mathbf{m}, t) = \sqrt{\frac{\sum_s (T_s(\mathbf{m}, t) - M_s(t))^2}{\sum_s M_s(t)^2}} + \rho \frac{\sum_{ij} \big(H_p(\phi_i, \lambda_j, t, F_p(\phi, \lambda, t, \mathbf{m}^f), \mathbf{m}^h) - H(\phi_i, \lambda_j, t, F_p(\phi, \lambda, t, \mathbf{m}^f))\big)^2}{\sum_{ij} H(\phi_i, \lambda_j, t, F_p(\phi, \lambda, t, \mathbf{m}^f))^2}, \tag{9}$$

where $T_s(\mathbf{m}, t)$ is the synthetic STEC calculated along s from the IRI-Plas for the given parameter set $\mathbf{m}$ at time t, $M_s(t)$ is the real STEC measurement obtained along s at time t, ϕ_i and λ_j are the discrete latitude and the longitude values spanning the region A with a step size of 1°, and ρ is an adjustable parameter which determines the penalty of the deviation from the physical relation between the f_0F_2 and the h_mF_2 parameters. A method for calculating synthetic STEC (T_s) values by using IRI-Plas model is given in Tuna et al. (2014). Notice that, the cost function and its parameters given in Tuna et al. (2015) are slightly modified in this paper. In the above defined criteria of optimization, deviation from the physical relation between f_0F_2 and h_mF_2 parameters given in IRI-Plas model has a quadratically increasing penalty. In an extensive set of reconstructions, it has been observed that this form produces more compliant results with the real measurements.

Among many existing alternatives, Broyden - Fletcher - Goldfarb - Shanno (BFGS) optimization algorithm which is found to provide the optimum set of parameters very efficiently (Tuna et al., 2015), is utilized to find the optimum $\mathbf{m}$ which minimizes $C(\mathbf{m}, t)$. The BFGS method uses both the first order derivatives and the second order derivatives of the problem space which are derived again from the first order derivatives, for finding the optimum solution. In the absence of a closed form analytical expression, the gradient is approximated by:

$$\nabla C(\mathbf{m}, t) = \sum_{d=1}^{n} \frac{C(\mathbf{m} + \epsilon \mathbf{z}_d, t) - C(\mathbf{m}, t)}{\epsilon} \mathbf{z}_d, \tag{10}$$

where $\{\mathbf{z}_d : 1 \leqslant d \leqslant n\}$ is an orthonormal basis for $\mathbb{R}^n$, and ϵ is a small positive real number.

The BFGS method uses the following iterations in its gradient based search:

$$\mathbf{B}_{t,k} \mathbf{p}_{t,k} = -\nabla C(\mathbf{m}_{t,k}, t), \tag{11}$$

$$\mathbf{m}_{t,k+1} = \mathbf{m}_{t,k} + \psi_{t,k} \mathbf{p}_{t,k}, \tag{12}$$

$$\mathbf{s}_{t,k} = \psi_{t,k} \mathbf{p}_{t,k}, \tag{13}$$

$$\mathbf{y}_{t,k} = \nabla C(\mathbf{m}_{t,k+1}, t) - \nabla C(\mathbf{m}_{t,k}, t), \tag{14}$$

$$\mathbf{B}_{t,k+1} = \mathbf{B}_{t,k} + \frac{\mathbf{y}_{t,k} \mathbf{y}_{t,k}^T}{\mathbf{y}_{t,k}^T \mathbf{s}_{t,k}} - \frac{\mathbf{B}_{t,k} \mathbf{s}_{t,k} \mathbf{s}_{t,k}^T \mathbf{B}_{t,k}}{\mathbf{s}_{t,k}^T \mathbf{B}_{t,k} \mathbf{s}_{t,k}}, \tag{15}$$

where k is the iteration count, $\psi_{t,k}$ is the step size parameter found by using a line search algorithm. $\mathbf{B}$ is the approximation of the Hessian matrix which is updated at each iteration. The initial value for $\mathbf{B}$ is used as the identity matrix. The starting point in the BFGS optimization method is set as the zero vector, which corresponds to the default IRI-Plas solution. The initial value of the step size is an exponentially decaying function with respect to the iteration number. The step size at each iteration is found by using a backtracking line search algorithm based on Armijo-Goldstein condition (Armijo, 1966) with a step size reduction ratio of 1/2.

Table 1
Planetary Wp Indices obtained from http://www.izmiran.ru/ionosphere/weather/storm/ for the days used in the experiments.

Date	UT																							Mean
	0	1	2	3	4	5	6	7	8	9	10	11	12	13	14	15	16	17	18	19	20	21	22	23	
2011.03.10	2.2	2.1	2.1	2.3	2.4	2.4	2.3	2.2	2.4	2.8	3.7	4.2	3.8	3.6	2.9	2.5	2.7	2.6	2.2	2.2	2.5	3.3	4.0	3.7	2.8
2011.05.28	2.9	3.0	3.3	3.4	3.8	3.8	3.8	3.7	4.2	4.9	5.4	5.7	5.8	5.7	5.4	5.3	4.9	4.6	4.4	4.2	4.2	3.6	3.2	3.4	4.3
2011.06.12	2.2	2.3	2.4	2.3	2.2	2.3	2.6	2.7	2.8	2.5	2.5	2.4	2.2	1.9	2.3	2.3	2.4	2.4	2.5	2.4	2.2	2.5	2.8	2.4	2.4
2011.09.01	2.3	2.0	2.0	2.0	2.1	2.3	2.3	2.2	2.3	2.1	2.3	2.0	2.5	2.6	2.9	3.1	3.1	3.0	2.7	2.9	2.7	2.5	2.3	2.3	2.4

The IONOLAB-CIT technique results are investigated for the following set of quiet and solar active days:

- 10 March 2011 (stormy day),
- 28 May 2011 (stormy day),
- 12 June 2011 (quiet day),
- 1 September 2011 (quiet day).

The planetary Wp indices (Gulyaeva and Stanislawska, 2008) for the selected days are given in the Table 1. A catalogue of TEC storms with Wp indices can be found at IZMIRAN Ionospheric Weather website of http://www.izmiran.ru/services/iweather/.

The reconstructions of the IONOLAB-CIT technique corresponding to these days generated the perturbation surface parameters that minimizes the cost function given in (9). Figs. 2–5 show the cost functions obtained by using the IRI-Plas and the IONOLAB-CIT and the corresponding perturbation surface parameters for 15 min time intervals. Independent runs of the IONOLAB-CIT on both quiet and stormy days show that the perturbation surface parameters are highly correlated in time. This result indicates that the perturbation surface parameters obtained from previous measurements can be utilized in a way to decrease the computation cost. Furthermore, the perturbation surface parameters can be tracked or even smoothed out in time for obtaining more robust results.

In this paper, the above described IONOLAB-CIT technique is extended to a space - time domain CIT technique. Unlike the IONOLAB-CIT, the 4D-IONOLAB-CIT exploits the temporal correlation of the ionosphere to provide improved reconstructions at any given time and on any time-interval of interest. The diagram of the 4D-IONOLAB-CIT technique is given in Fig. 1.

3. Investigation of temporal correlation in the CIT results

In the previous section, it is observed that there is a high temporal correlation of perturbation surface parameters obtained by using the IONOLAB-CIT technique. Therefore, the ionospheric tomography results can be improved if the observed temporal continuity of the parameters are exploited. In this section, the temporal correlation in the CIT results is investigated further. A state transition model is defined for predicting the future perturbation surface parameters from previous results. The state of the system at time t is denoted by the vector $\mathbf{m}_t$, which contains the perturbation surface parameters provided by the IONOLAB-CIT technique at time t. The state transition model is assumed to be linear and time independent, thus it is expressed as a matrix denoted by $\mathbf{F}$. The state transition noise process at time t is denoted by $\mathbf{w}_t$. The state transition equation can be written as follows:

$$\mathbf{m}_t = \mathbf{F}\mathbf{m}_{t-1} + \mathbf{w}_t. \tag{16}$$

Since the physical structure of the underlying model is not known, three different approaches for defining state transition model are proposed. In all cases, the state transition model is assumed to be linear, thus they are defined as state transition matrices.

In the first model, it is assumed that the ionospheric perturbation surfaces are highly correlated in time and stay constant with respect to the geodetic coordinate system. In this case, the state transition matrix is defined as the identity matrix.

$$\mathbf{F}_1 = \mathbf{I}_{6\times 6}. \tag{17}$$

In the second model, it is assumed that the ionospheric perturbation surfaces are highly correlated in time and stay constant with respect to the position of the sun. In this case, the state transition matrix is defined as the following:

$$\mathbf{F}_2 = \begin{bmatrix} 1 & 0 & 0 & 0 & 0 & 0 \\ 0 & 1 & 0 & 0 & 0 & 0 \\ 0 & \frac{2}{\lambda_{max}-\lambda_{min}}\frac{360}{24}\Delta t & 1 & 0 & 0 & 0 \\ 0 & 0 & 0 & 1 & 0 & 0 \\ 0 & 0 & 0 & 0 & 1 & 0 \\ 0 & 0 & 0 & 0 & \frac{2}{\lambda_{max}-\lambda_{min}}\frac{360}{24}\Delta t & 1 \end{bmatrix}, \tag{18}$$

where λ_{min} and λ_{max} represent the minimum and maximum values of longitude in the region of interest, respectively, and Δt represents the time interval in hours.

In the third model, by using the results obtained from the IONOLAB-CIT, a linear regression analysis method is used to find a state transition matrix that produces the minimum mean square error. Linear regression method tries to find the optimum linear relation between a dependent variable and one or more independent variables. The dependent variable can be predicted by using the obtained linear relation model and the independent variable(s). In the regression analysis, the perturbation surface parameters calculated by the IONOLAB-CIT are used as dependent variables, and the perturbation surface parameters calculated by the IONOLAB-CIT corresponding to the previous time instant are used as the independent variables. Let $\mathbf{m}_t$ denote the array containing the perturbation surface parameters calculated by the IONOLAB-CIT technique at time t, and $m_{t,n}$ denote the nth parameter in $\mathbf{m}_t$. The corresponding regression model can be written as follows:

$$\mathbf{a_n} = \mathbf{X}\mathbf{f}_n + \epsilon_\mathbf{n}, \tag{19}$$

where $\epsilon_\mathbf{n}$ is the error term, and $\mathbf{a_n}$ and $\mathbf{X}$ are defined as:

$$\mathbf{a_n} = \begin{bmatrix} m_{1,n} \\ m_{2,n} \\ \cdots \\ m_{t,n} \end{bmatrix}, \tag{20}$$

$$\mathbf{X} = \begin{bmatrix} \mathbf{m}_0^T \\ \mathbf{m}_1^T \\ \cdots \\ \mathbf{m}_{t-1}^T \end{bmatrix}. \tag{21}$$

The least squares estimation for $\mathbf{f}_n$ can be found by using the following equation:

$$\hat{\mathbf{f}}_n = \left(\mathbf{X}^T\mathbf{X}\right)^{-1}\mathbf{X}^T\mathbf{a_n}. \tag{22}$$

The state transition matrix found by the linear regression method can be written as $\mathbf{F}_3 = \begin{bmatrix} \hat{\mathbf{f}}_0 & \hat{\mathbf{f}}_1 & \hat{\mathbf{f}}_2 & \hat{\mathbf{f}}_3 & \hat{\mathbf{f}}_4 & \hat{\mathbf{f}}_5 \end{bmatrix}^T$.

The state transition matrices found by the linear regression method for days 10 March 2011, 28 May 2011, 12 June 2011 and 1 September 2011 are given in Table 2.

Figs. 6–11 show the cost functions obtained for the predicted perturbation parameters for each state transition matrix and for increasingly longer time intervals, for 28 May 2011 and 12 June 2011.

Obtained results show that the state transition matrices $\mathbf{F}_1$ and $\mathbf{F}_3$ produce similar estimates, which are better than those provided by $\mathbf{F}_2$. This result indicates that using previous disturbance surfaces which are obtained over the same region defined in geodetic coordinates produce better

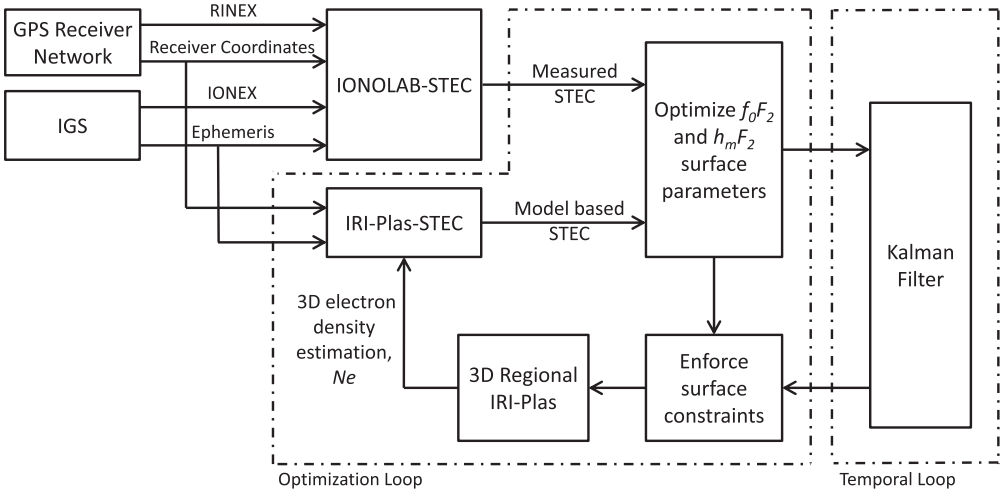

Fig. 1. 4D-IONOLAB-CIT.

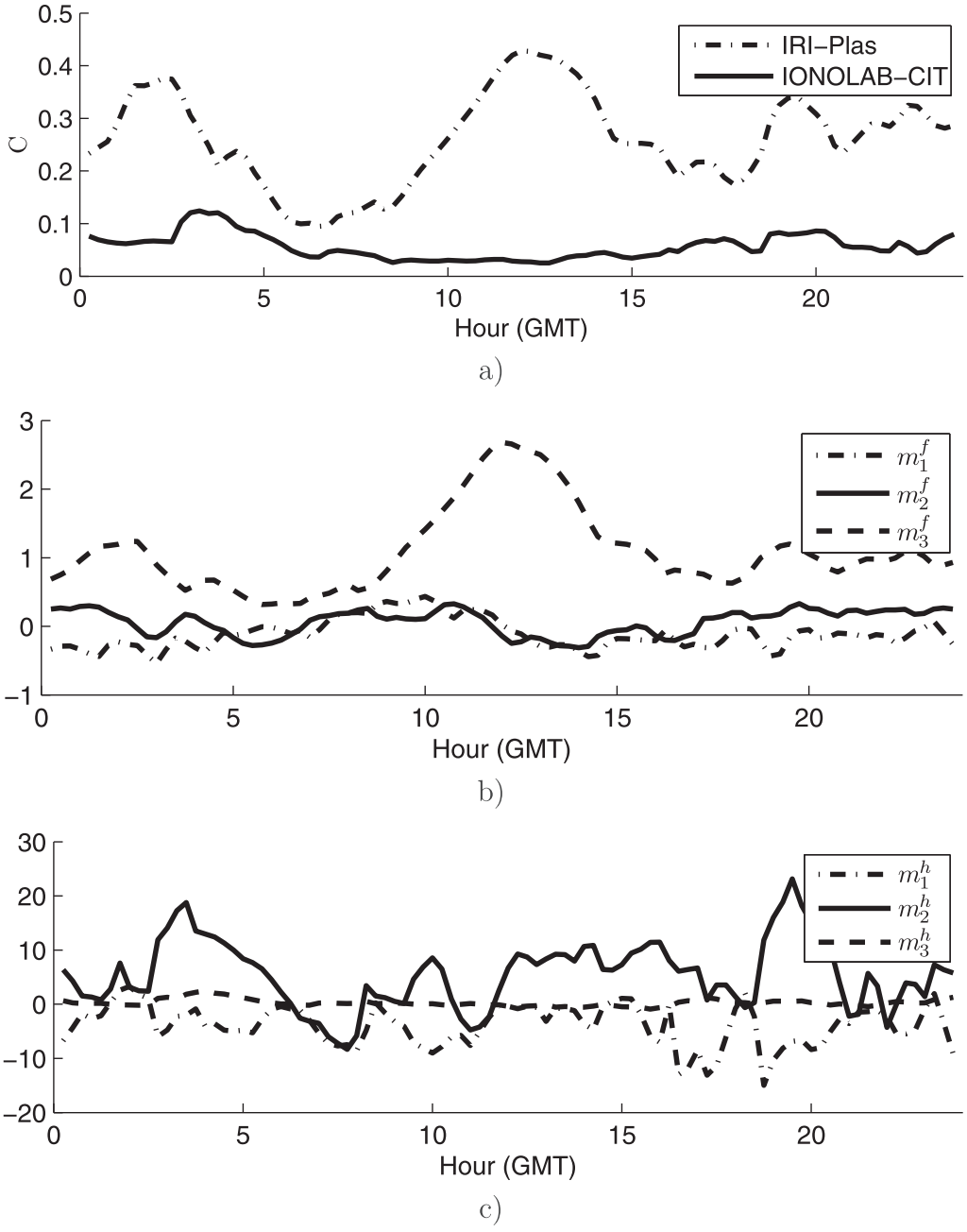

Fig. 2. Results obtained by the IONOLAB-CIT technique on 10 March 2011. (a) Comparison of cost functions obtained by IRI-Plas and IONOLAB-CIT, (b) f_0F_2 perturbation surface parameters, (c) h_mF_2 perturbation surface parameters.

estimates than rotating them with respect to the sun zenith angle. Results also show that the temporal validity of the CIT results obtained by using the IONOLAB-CIT decreases as the time interval between the measurements and the predictions get longer, and after time interval reaches to certain values, using previous results may increase the cost function above the cost value obtained by using the default IRI-Plas parameters. Figs. 12–15 contain the average cost values obtained by using the state transition matrices $\mathbf{F}_1, \mathbf{F}_2$ and $\mathbf{F}_3$ for increasingly longer intervals, and their comparison with IONOLAB-CIT and IRI-Plas results. Results indicate that, in the case of $\mathbf{F}_1$, using the predicted perturbation surface parameters produces better results than using the default IRI-Plas parameters even for a 3 h interval for days 10 March 2011, 12 June 2011 and 1 September 2011. On 28 May 2011, using the predicted perturbation surface parameters produces better results than using the default IRI-Plas parameters up to 1 h interval. Based on the results, it can be concluded that predicting future perturbation surface parameters by using the state transition matrix $\mathbf{F}_1$ on the previous IONOLAB-CIT results obtained up to 1 h ago produces better results than using the IRI-Plas model directly. Results also show that, the state transition matrix $\mathbf{F}_1$

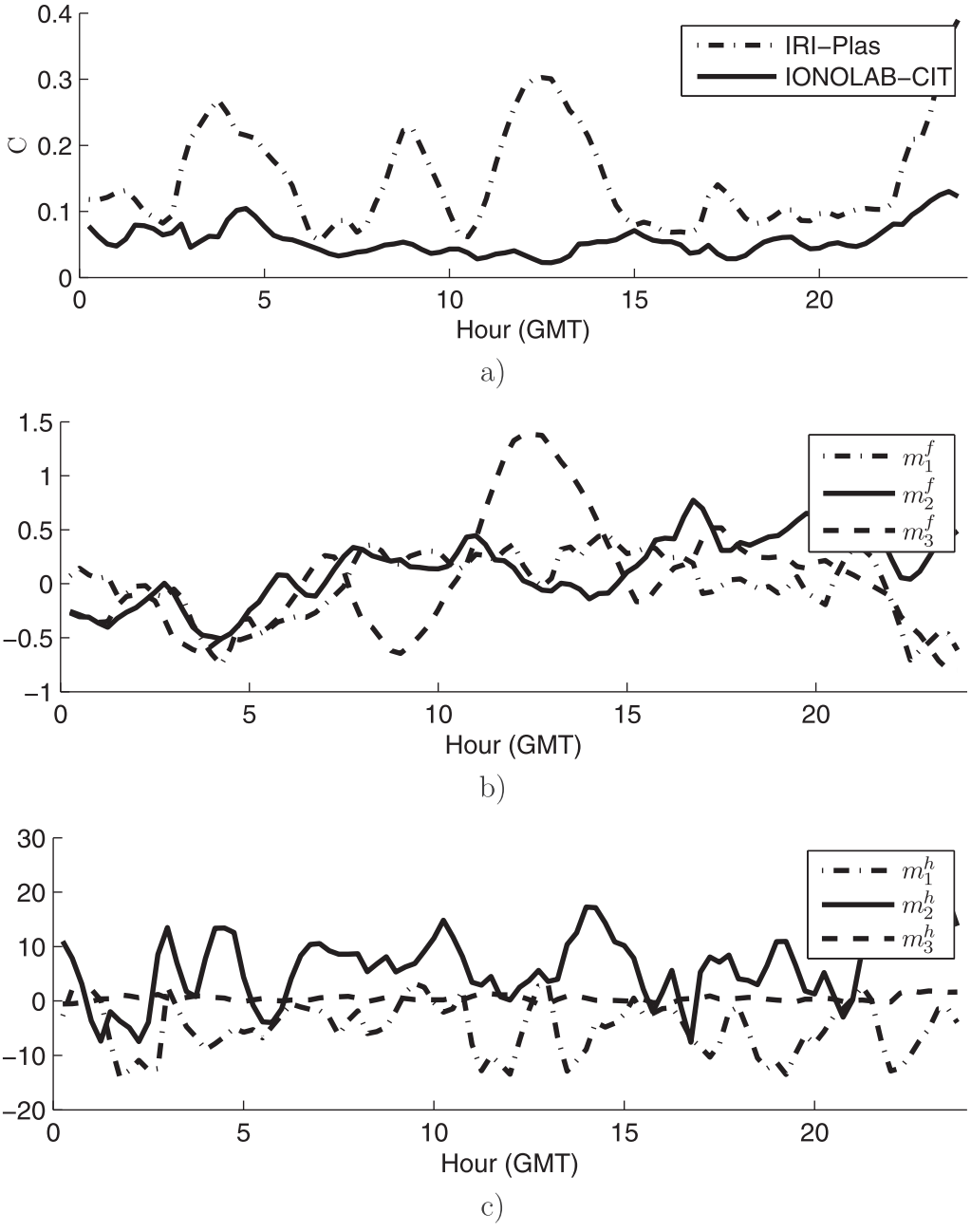

Fig. 3. Results obtained by the IONOLAB-CIT technique on 28 May 2011. (a) Comparison of cost functions obtained by IRI-Plas and IONOLAB-CIT, (b) f_0F_2 perturbation surface parameters, (c) h_mF_2 perturbation surface parameters.

produces very similar results to $\mathbf{F}_3$, which is the optimum matrix in terms of the MMSE estimation.

4. Kalman filtering of the perturbation parameters in time

In order to track perturbation surface parameters in time, a Kalman filtering based approach is implemented over the sequence of perturbation surface parameters (Kalman, 1960). Use of Kalman filtering increases the robustness and accuracy of the proposed CIT technique.

In our application of the Kalman filter, the state of the system at time instant t is represented as the vector $\mathbf{m}_t$ containing perturbation surface parameters, the state transition matrix is time independent and is represented as $\mathbf{F}$, and there is no control input to the system. The state update equation is given as:

$$\mathbf{m}_t = \mathbf{F}\mathbf{m}_{t-1} + \mathbf{w}_t. \tag{23}$$

where $\mathbf{w}_t$ represents the state transition noise at time instant t. The observable parameter of the system is the perturbation surface parameters estimated by the IONOLAB-CIT technique, and it is related to the system state via the following equation:

$$\mathbf{z}_t = \mathbf{m}_t + \mathbf{v}_t, \tag{24}$$

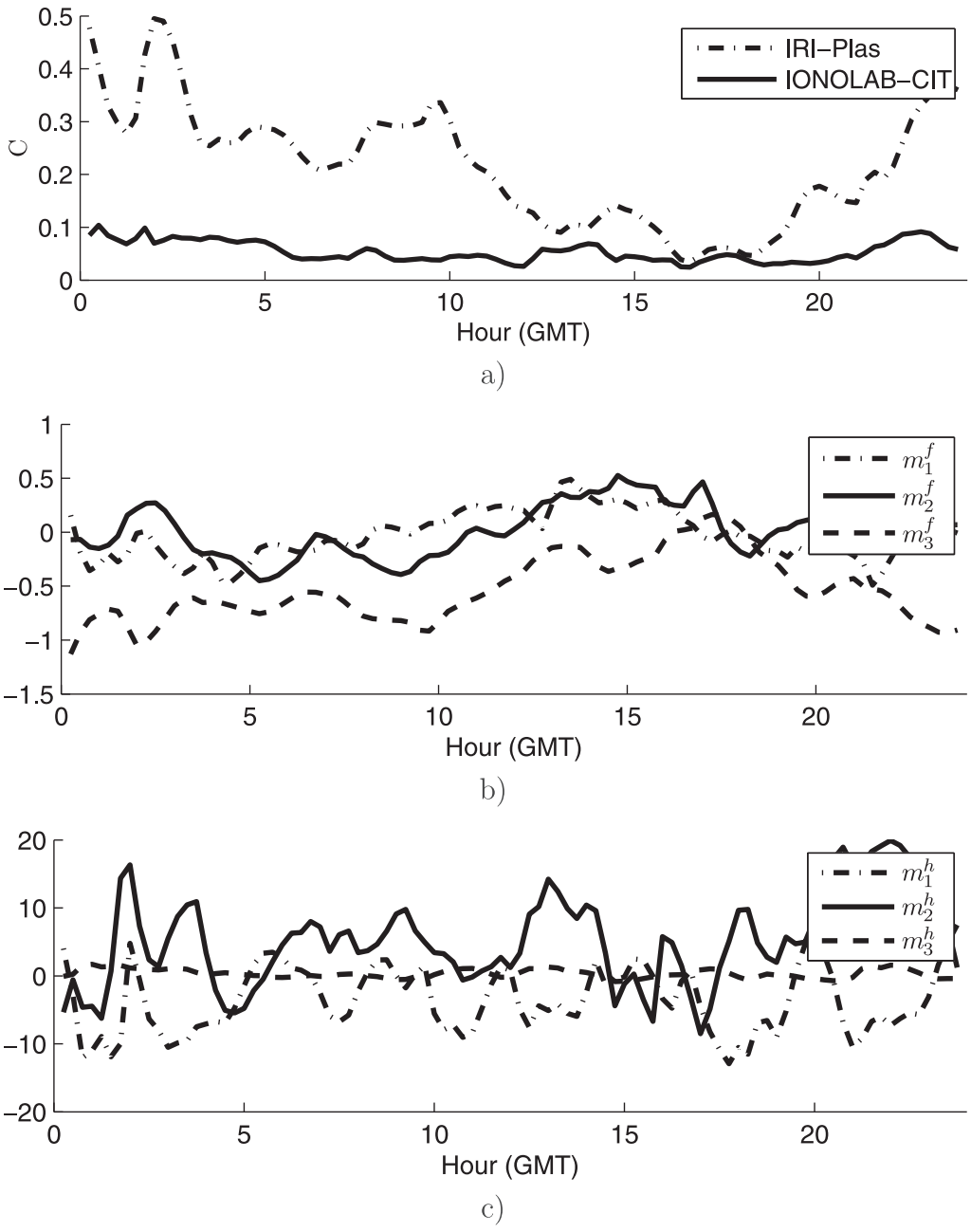

Fig. 4. Results obtained by the IONOLAB-CIT technique on 12 June 2011. (a) Comparison of cost functions obtained by IRI-Plas and IONOLAB-CIT, (b) f_0F_2 perturbation surface parameters, (c) h_mF_2 perturbation surface parameters.

where $\mathbf{z}_t$ is the observation, and $\mathbf{v}_t$ is the observation noise at time instant t. Since the perturbation parameters are uncorrelated with each other, the state transition and the observation noise processes are selected as:

$$\mathbf{w}_t \sim N(0, \mathbf{Q}), \tag{25}$$

$$\mathbf{Q} = q\mathbf{I}_{6\times 6}, \tag{26}$$

$$\mathbf{v}_t \sim N(0, \mathbf{R}), \tag{27}$$

$$\mathbf{R} = r\mathbf{I}_{6\times 6}. \tag{28}$$

After determining the state transition and the observation models of the system, Kalman filter prediction and update phases can be written as:

Prediction:

$$\hat{\mathbf{m}}_{t|t-1} = \mathbf{F}\hat{\mathbf{m}}_{t-1|t-1}, \tag{29}$$

$$\mathbf{P}_{t|t-1} = \mathbf{F}\mathbf{P}_{t-1|t-1}\mathbf{F}^T + \mathbf{Q}. \tag{30}$$

Update:

$$\hat{\mathbf{y}}_t = \mathbf{z}_t - \hat{\mathbf{m}}_{t|t-1}, \tag{31}$$

$$\mathbf{S}_t = \mathbf{P}_{t|t-1} + \mathbf{R}, \tag{32}$$

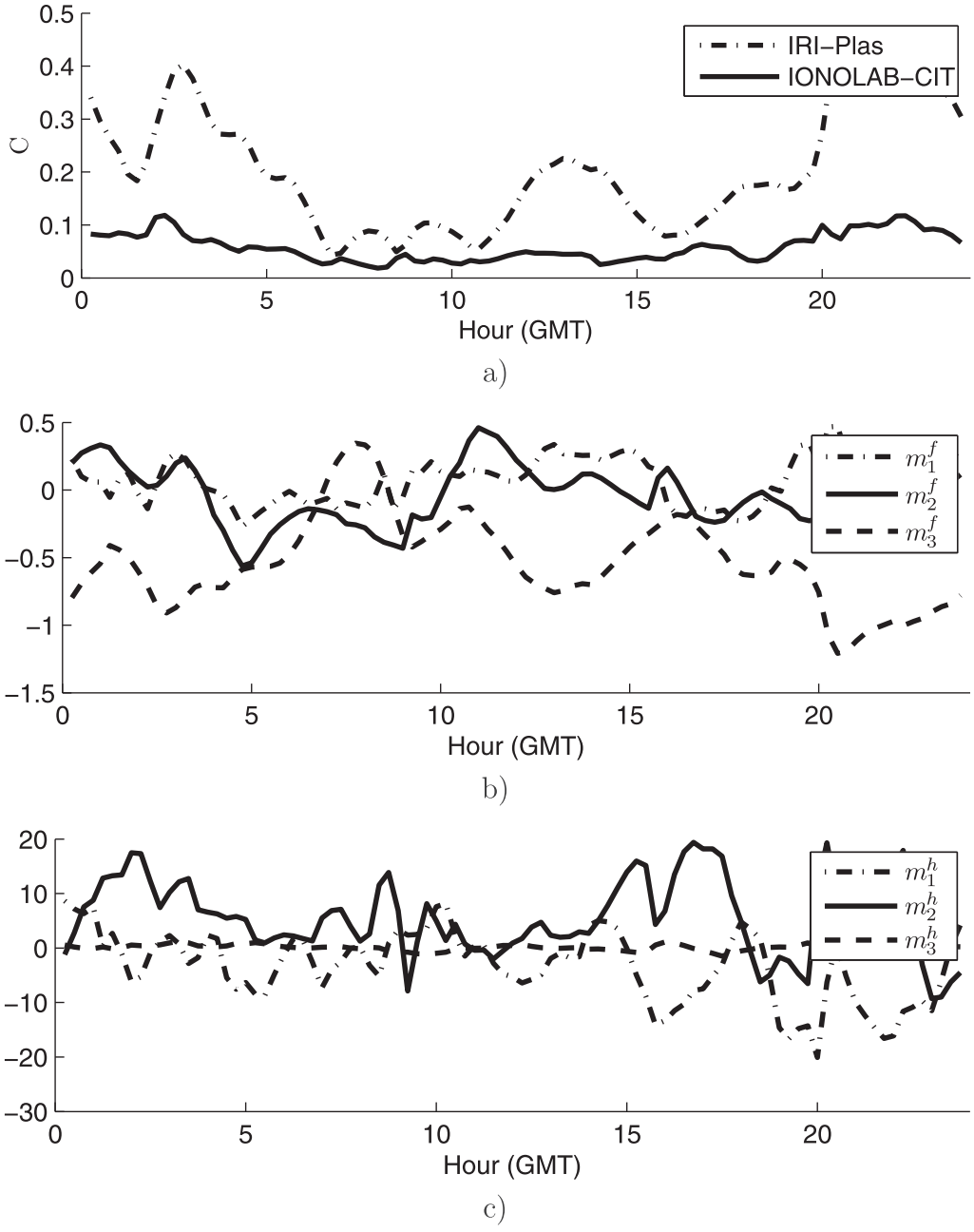

Fig. 5. Results obtained by the IONOLAB-CIT technique on 1 September 2011. (a) Comparison of cost functions obtained by IRI-Plas and IONOLAB-CIT, (b) f_0F_2 perturbation surface parameters, (c) h_mF_2 perturbation surface parameters.

$$\mathbf{K}_t = \mathbf{P}_{t|t-1}\mathbf{S}_t^{-1}, \tag{33}$$

$$\hat{\mathbf{m}}_{t|t} = \hat{\mathbf{m}}_{t|t-1} + \mathbf{K}_t\hat{\mathbf{y}}_t, \tag{34}$$

$$\mathbf{P}_{t|t} = (\mathbf{I} - \mathbf{K}_t)\mathbf{P}_{t|t-1}. \tag{35}$$

The noise coefficients q and r determine the reliance on the state transition model or the measurements, i.e., the IONOLAB-CIT results. In this scenario, the ratio of q and r, rather than their exact values, is important for Kalman filtering results.

5. Kalman smoothing of the perturbation surface parameters in time

Kalman filtering approach produces estimates depending on the current and previous observations, and it is the optimum causal filtering when the system and observation noises are Gaussian-distributed. However, it is possible to smooth the estimates further by using the off-line Kalman smoothing technique. In order to do that, the

Table 2
The state transition matrices found by the linear regression method for days 10 March 2011, 28 May 2011, 12 June 2011 and 1 September 2011.

10 March 2011	0.894	0.044	−0.022	−0.002	0.000	−0.001
	−0.019	0.933	−0.024	−0.005	0.001	−0.016
	0.166	0.243	1.021	0.000	−0.004	0.027
	−1.611	−0.190	−0.619	0.729	−0.026	−0.442
	−2.209	−0.780	0.972	0.011	0.770	0.596
	−0.073	0.023	−0.008	0.002	0.005	0.889
28 May 2011	0.903	0.004	0.059	0.004	0.000	0.020
	−0.033	0.983	−0.011	0.000	0.000	0.005
	−0.000	0.056	0.981	0.002	−0.005	0.041
	−0.480	−0.732	−0.085	0.833	−0.027	−0.016
	−0.550	1.733	0.388	−0.074	0.812	1.313
	−0.105	0.086	−0.073	−0.015	0.005	0.708
12 June 2011	0.937	−0.060	0.038	0.004	0.002	0.053
	0.056	0.899	0.015	0.003	0.003	0.021
	0.053	0.057	0.933	0.004	−0.004	0.011
	0.630	−2.586	1.404	0.814	0.065	0.044
	−2.060	1.251	−0.418	−0.135	0.833	−0.039
	−0.251	0.276	−0.113	−0.015	−0.008	0.744
1 September 2011	0.821	−0.016	−0.031	−0.002	−0.002	−0.026
	0.061	0.924	−0.017	−0.000	−0.001	−0.052
	−0.048	−0.008	0.942	0.005	−0.002	0.016
	0.289	−0.477	1.175	0.822	0.044	−0.534
	5.965	−0.971	1.381	−0.029	0.904	3.113
	−0.105	0.226	−0.144	−0.000	−0.007	0.728

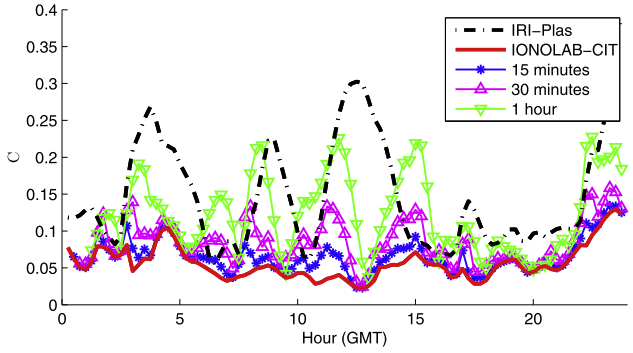

Fig. 6. Cost functions of the perturbation surface parameters predicted by using the state transition matrix $\mathbf{F}_1$ for increasingly longer time intervals, on 28 May 2011.

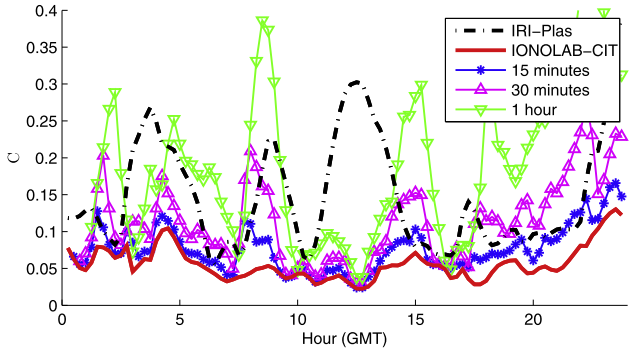

Fig. 7. Cost functions of the perturbation surface parameters predicted by using the state transition matrix $\mathbf{F}_2$ for increasingly longer time intervals, on 28 May 2011.

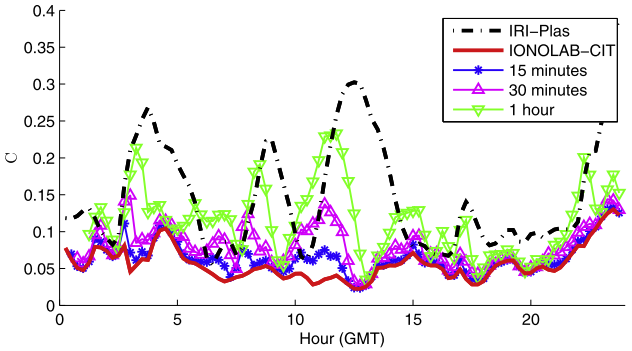

Fig. 8. Cost functions of the perturbation surface parameters predicted by using the state transition matrix $\mathbf{F}_3$ for increasingly longer time intervals, on 28 May 2011.

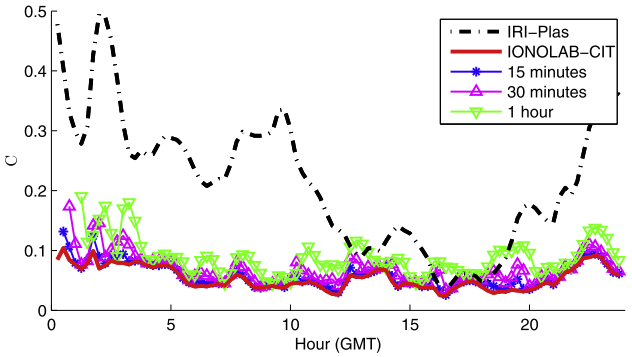

Fig. 9. Cost functions of the perturbation surface parameters predicted by using the state transition matrix $\mathbf{F}_1$ for increasingly longer time intervals, on 12 June 2011.

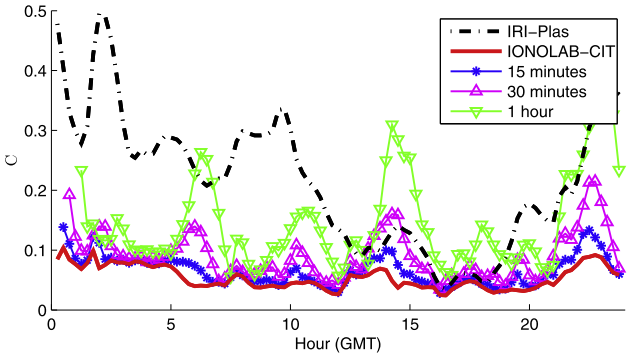

Fig. 10. Cost functions of the perturbation surface parameters predicted by using the state transition matrix $\mathbf{F}_2$ for increasingly longer time intervals, on 12 June 2011.

Rauch-Tung-Striebel smoother, which is basically a two-pass algorithm based on the Kalman filter approach is implemented in this paper (Rauch et al., 1965). This smoother works by applying forward and backward passes on the estimated perturbation surface parameters. Forward pass is the same as the Kalman filtering approach, however, the state estimations and covariance matrices are stored to be used in the backward pass. The backward pass is performed by the following recursive equations:

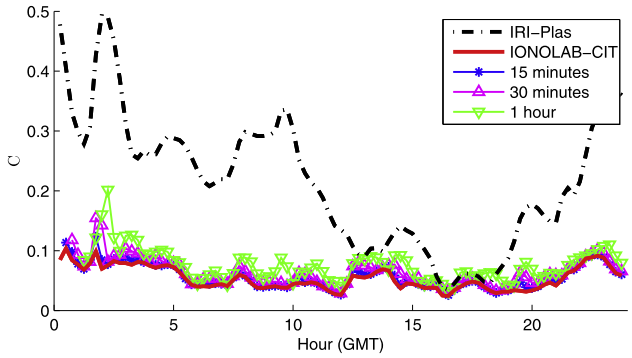

Fig. 11. Cost functions of the perturbation surface parameters predicted by using the state transition matrix $\mathbf{F}_3$ for increasingly longer time intervals, on 12 June 2011.

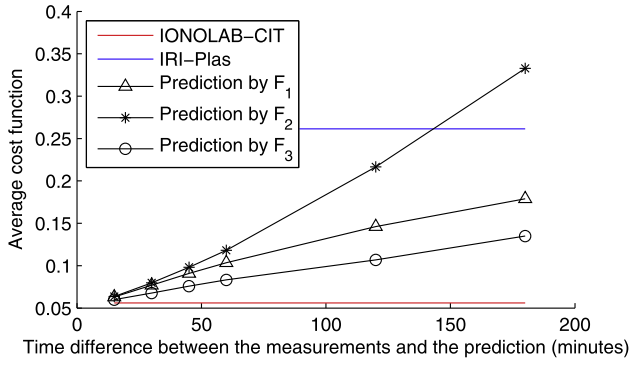

Fig. 12. Average cost values obtained by using $\mathbf{F}_1, \mathbf{F}_2$ and $\mathbf{F}_3$ state transition matrices for increasingly longer time intervals, and their comparison with IONOLAB-CIT and IRI-Plas results, on 10 March 2011.

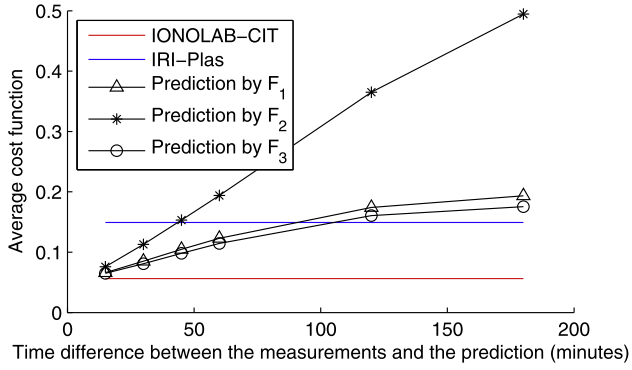

Fig. 13. Average cost values obtained by using $\mathbf{F}_1, \mathbf{F}_2$ and $\mathbf{F}_3$ state transition matrices for increasingly longer time intervals, and their comparison with IONOLAB-CIT and IRI-Plas results, on 28 May 2011.

$$\hat{\mathbf{m}}_{t|n} = \hat{\mathbf{m}}_{t|t} + \mathbf{C}_t(\hat{\mathbf{m}}_{t+1|n} - \hat{\mathbf{m}}_{t+1|t}), \tag{36}$$

$$\mathbf{P}_{t|n} = \mathbf{P}_{t|t} + \mathbf{C}_t(\mathbf{P}_{t+1|n} - \mathbf{P}_{t+1|t})\mathbf{C}_t^T, \tag{37}$$

where n is the total number of observations, and $\mathbf{C}$ is defined as:

$$\mathbf{C}_t = \mathbf{P}_{t|t}\mathbf{F}^T\mathbf{P}_{t+1|t}^{-1}. \tag{38}$$

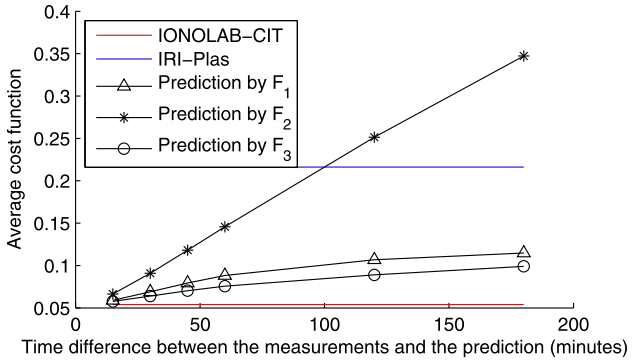

Fig. 14. Average cost values obtained by using $\mathbf{F}_1, \mathbf{F}_2$ and $\mathbf{F}_3$ state transition matrices for increasingly longer time intervals, and their comparison with IONOLAB-CIT and IRI-Plas results, on 12 June 2011.

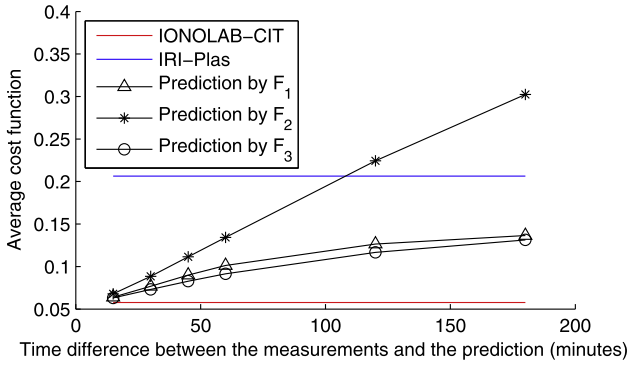

Fig. 15. Average cost values obtained by using $\mathbf{F}_1, \mathbf{F}_2$ and $\mathbf{F}_3$ state transition matrices for increasingly longer time intervals, and their comparison with IONOLAB-CIT and IRI-Plas results, on 1 September 2011.

It is possible to use Kalman smoothing approach on-line as a non-causal filter for better estimations. As the new measurements are obtained, the previous estimations can be further corrected after some time delay.

6. Results

In the following simulations, the state transition matrix is used as $\mathbf{F}_1$, the state transition noise $\mathbf{Q}$ is selected as $0.2\mathbf{I}$, and the measurement noise $\mathbf{R}$ is selected as $0.1\mathbf{I}$. The region of reconstruction is selected in between 34°N and 44°N latitudes, 24°E and 47°E longitudes, and 100 and 20,000 km in height. The real GPS-STEC measurements computed by the IONOLAB-STEC method from the data obtained from TNGPN-Active stations are used in the experiments (Nayir et al., 2007). Three different sets of experiments are carried out by using the Kalman filtering and the Kalman smoothing methods. Each experiment explained in detail and obtained results are given below.

In the first set of experiments, data from all available TNPGN-Active GPS receiver stations (total of 146 stations) are used, and all of the results obtained by the IONOLAB-CIT technique within 24 h are used in the

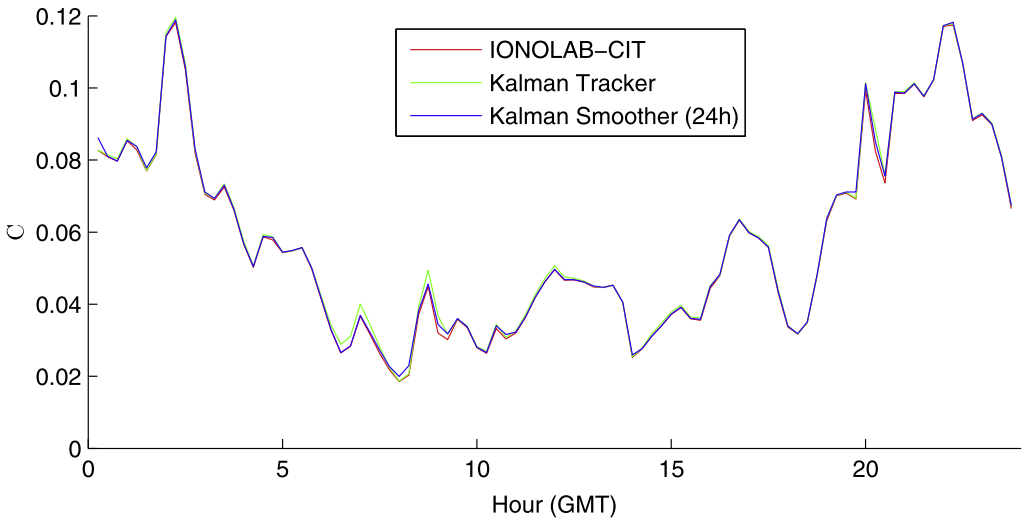

Fig. 16. Cost function obtained for independent runs of IONOLAB-CIT, and cost function obtained after application of Kalman filtering based tracking and Kalman smoothing methods on 1 September 2011, when all GPS receiver stations are used in reconstructions.

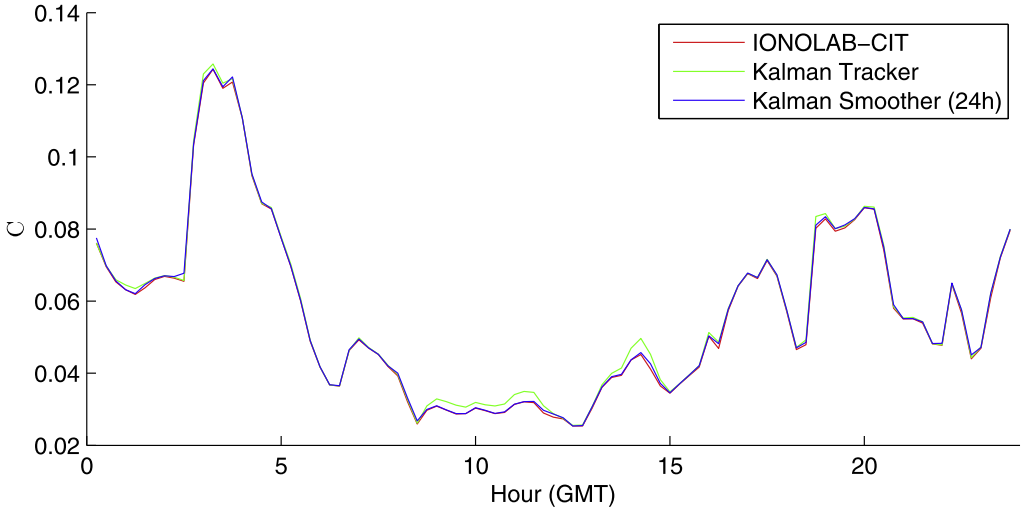

Fig. 17. Cost function obtained for independent runs of IONOLAB-CIT, and cost function obtained after application of Kalman filtering based tracking and Kalman smoothing methods on 10 March 2011, when all GPS receiver stations are used in reconstructions.

observation set of the Kalman smoothing method. Figs. 16 and 17 show cost functions obtained by using the Kalman filtering/smoothing methods on 1 September 2011 and 10 March 2011, compared with the IONOLAB-CIT results, which are obtained independently. Since the IONOLAB-CIT technique minimizes the cost function independently from the previous results, it achieves the minimum cost function. Using the Kalman filtering/smoothing on the results slightly increases this cost. However, using independent IONOLAB-CIT runs for each time instant may suffer from over fitting in the presence of noisy data. Therefore, obtaining the minimum cost function does not necessarily mean obtaining the most robust result. Figs. 18 and 19 show electron density slices along the latitude 39°N, obtained by using Kalman filtering method on 1 September 2011 and 10 March 2011, at 06:00, 12:00 and 18:00 GMT. Electron density values clearly depict the disturbance on 10 March 2011 at 12:00 GMT.

In the second set of experiments, only 3 TNPGN-Active GPS receiver stations spread over Turkey (*feth* (36.62°N, 29.12°E), *anrk* (39.85°N, 32.84°E) and *mard* (37.31°N, 40.72°E)) are used in the IONOLAB-CIT reconstruction set with the Kalman filtering and smoothing methods. All of the results obtained by the IONOLAB-CIT technique within 24 h are used in the observation set of the Kalman smoothing method. Figs. 20 and 21 show results obtained by using 3 GPS receiver stations on 1 September 2011 and 10 March 2011, with and without using the Kalman filtering/smoothing approaches. Results show that the cost function obtained with and without using Kalman filtering approaches are very similar in most cases. However, for the problematic cases where the IONOLAB-CIT produces

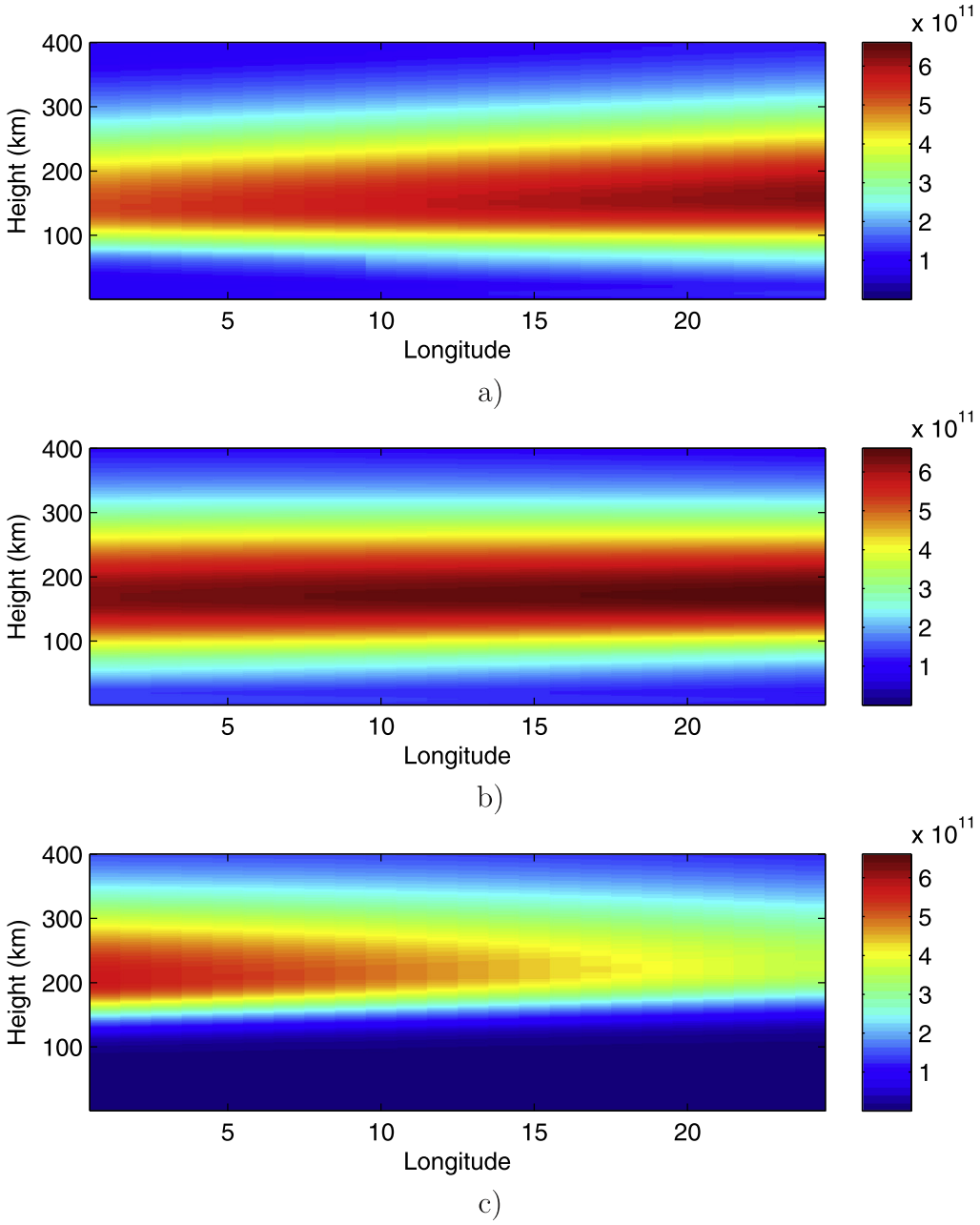

Fig. 18. Electron density slices in terms of electrons/m^3 obtained by using Kalman filtering on latitude 39°N, on 1 September 2011, at (a) 06:00, (b) 12:00, (c) 18:00 GMT.

significantly high cost values with respect to the full GPS receiver station set experiments, Kalman filtering and smoothing approaches produce better cost values. This result can be interpreted as that using Kalman filtering/smoothing methods increases the robustness of the results obtained by the IONOLAB-CIT technique, especially when the data from a few GPS receiver stations are used in the reconstruction.

In the third set of experiments, 3 TNPGN-Active GPS receiver stations (*feth*, *anrk* and *mard*) are used with the Kalman smoothing method for different observation set sizes in time. The Kalman smoothing method is run by using all results obtained by the IONOLAB-CIT technique up to 15 min into the future, and the results are compared with the performance of the Kalman smoothing method when all of the results obtained by the IONOLAB-CIT technique within 24 h are used. Figs. 22 and 23 show results obtained by using 3 GPS receiver stations on 1 September 2011 and 10 March 2011. Results show that the performance difference between two cases is very small, which indicates that using the Kalman smoothing method on-line with 15 min delay is sufficient for exploiting the advantage of the Kalman smoothing method.

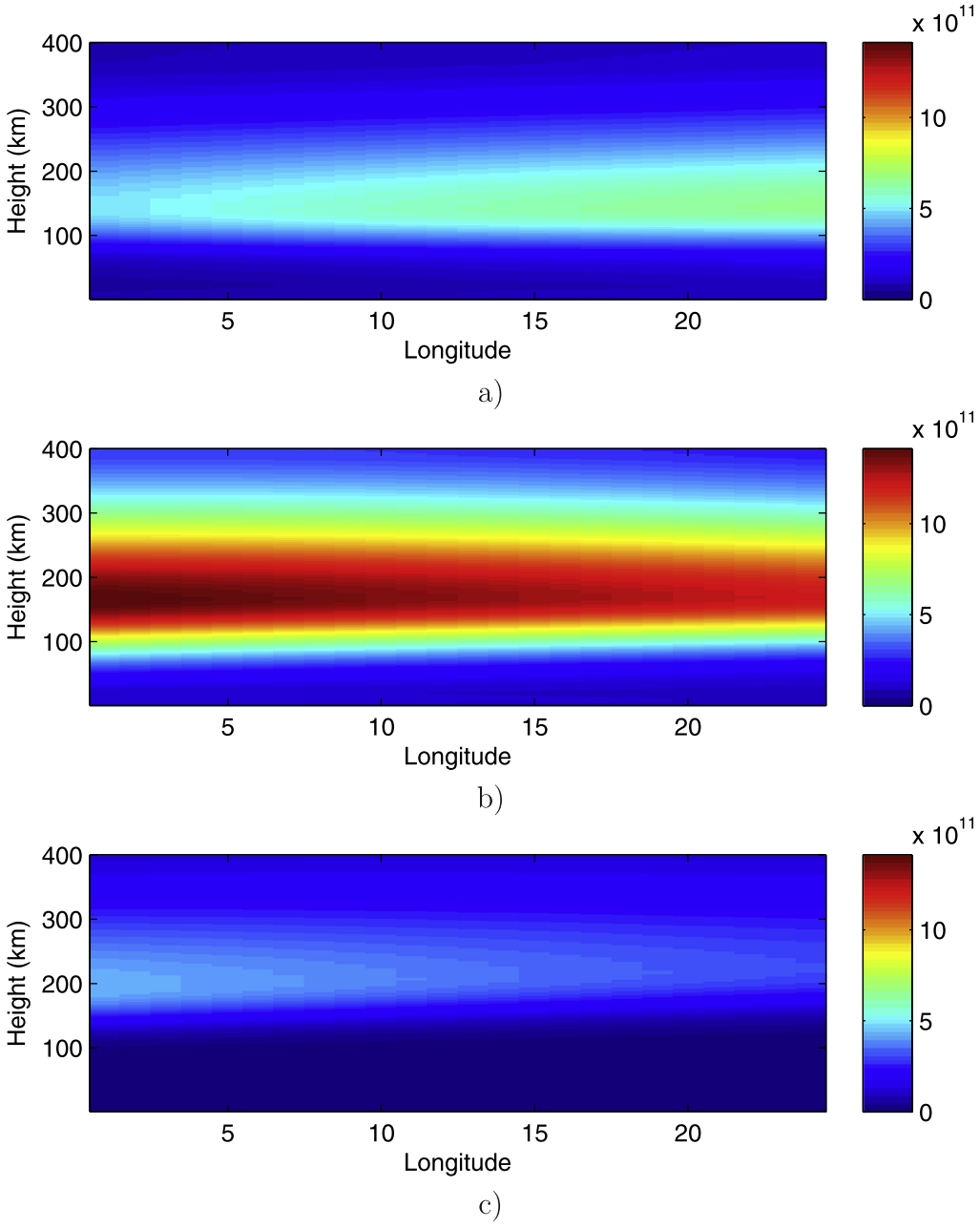

Fig. 19. Electron density slices in terms of electrons/m^3 obtained by using Kalman filtering on latitude 39°N, on 10 March 2011, at (a) 06:00, (b) 12:00, (c) 18:00 GMT.

7. Computational cost analysis

When using the IONOLAB-CIT technique, the state transition equation can be used for estimating the initial search point in the problem space of the next time instant. This process not only decreases the computational cost of the IONOLAB-CIT technique, but also starts the optimization search in a closer neighbourhood of the solution and decreases the probability of converging to the local minima in the problem space. In order to present a metric about the computational cost advantage of this method, average value of the initial cost functions obtained by using the default IRI-Plas parameters C_I, and the average value of the cost functions for predicted perturbation surface parameters C_T are given in Table 3. The average decrement in the computational cost is calculated by dividing the average number of iterations for decreasing the cost function from C_I to C_T, which will be denoted with K_D, by the average number of iterations for convergence when using the default IRI-Plas parameters, which will be denoted as K_C. Results indicate an average decrease between 16% and 20% in the computational cost. Note that, these results

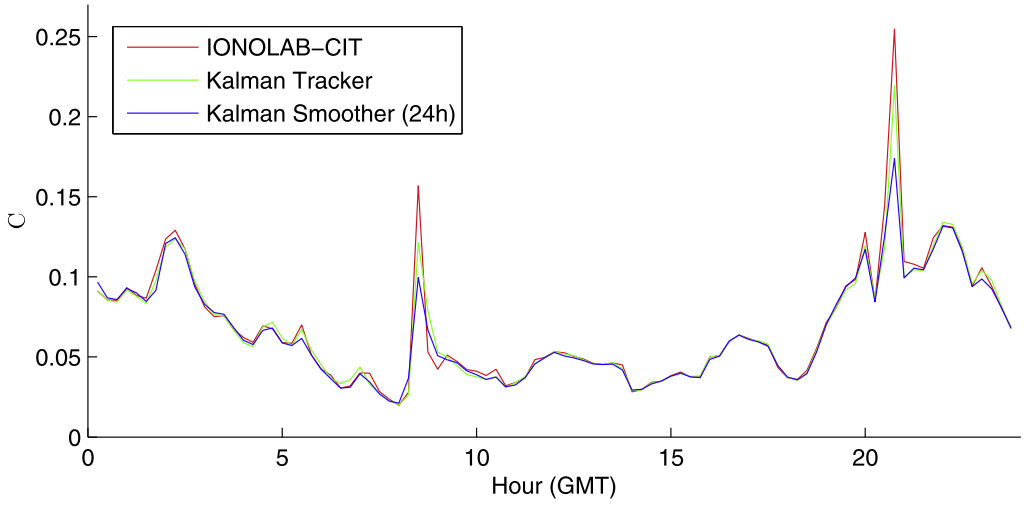

Fig. 20. Cost function obtained for independent runs of IONOLAB-CIT, and cost function obtained after application of Kalman filtering based tracking and Kalman smoothing methods on 1 September 2011, when 3 GPS receiver stations are used in reconstructions.

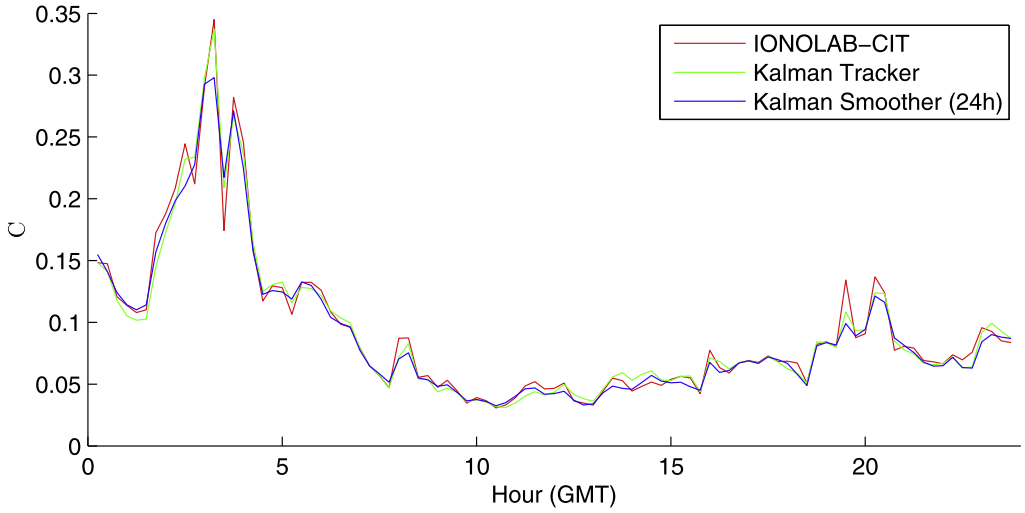

Fig. 21. Cost function obtained for independent runs of IONOLAB-CIT, and cost function obtained after application of Kalman filtering based tracking and Kalman smoothing methods on 10 March 2011, when 3 GPS receiver stations are used in reconstructions.

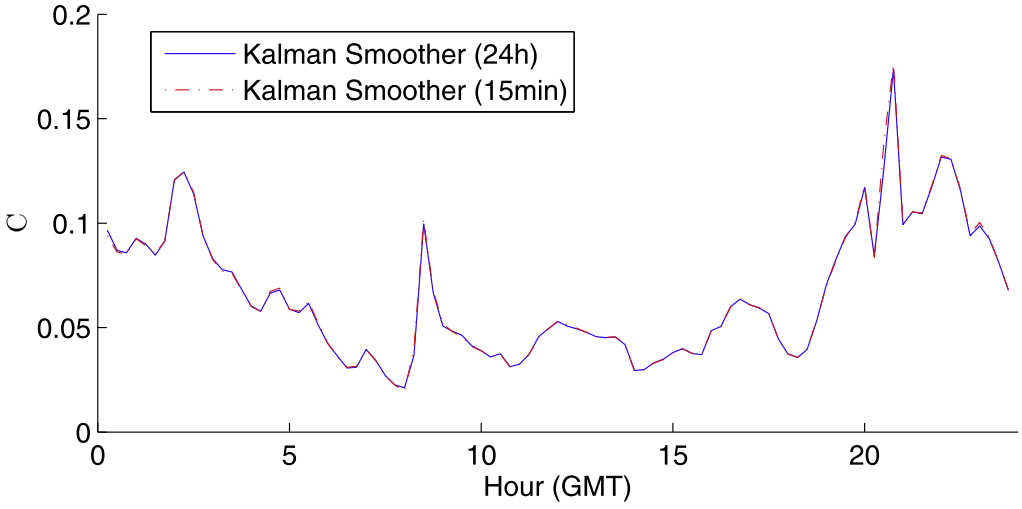

Fig. 22. Kalman smoothing results on 1 September 2011, when 3 GPS receiver stations are used in reconstructions, by using all results obtained by the IONOLAB-CIT technique up to 15 min into the future, and by using all results obtained by the IONOLAB-CIT technique within 24 h.

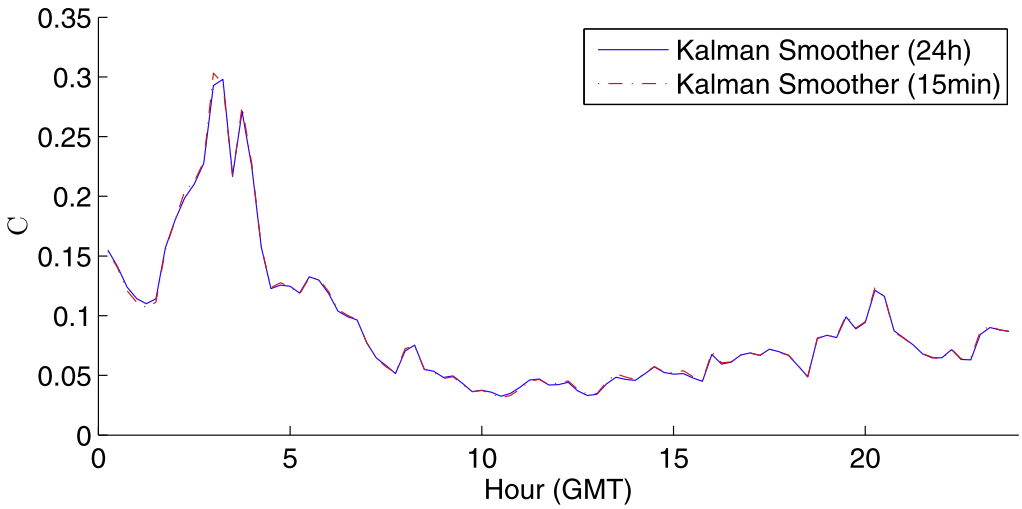

Fig. 23. Kalman smoothing results on 10 March 2011, when 3 GPS receiver stations are used in reconstructions, by using all results obtained by the IONOLAB-CIT technique up to 15 min into the future, and by using all results obtained by the IONOLAB-CIT technique within 24 h.

Table 3
Computational cost advantage of using Kalman prediction step for the next initial point in the IONOLAB-CIT technique.

Date	C_I	C_T	K_D	K_C	Computational Saving
1 September 2011	0.205	0.064	28.18	5.20	18.5%
10 March 2011	0.262	0.063	27.96	5.69	20.4%
28 May 2011	0.150	0.066	29.71	4.88	16.4%
12 June 2011	0.213	0.059	28.57	5.72	20.0%

are obtained for very strict stopping criteria for the BFGS method (solution candidate point in 6D space has moved less than 10^{-3} and the cost function has changed less than 10^{-4} in the last 3 iterations). If the stopping criteria is relaxed, the computational cost advantage of using the predicted perturbation surface parameters in terms of percentage will increase significantly.

8. Conclusions

In order to have 3-D distribution of electron density in the ionosphere, various Computerized Ionospheric Tomography (CIT) techniques have been proposed. In this study, a novel CIT technique, 4D-IONOLAB-CIT, that provides 3-D tomographic reconstruction results over a geographical region in a time-window of interest by exploiting temporal continuity of the electron density distribution in time, is presented. In 4D-IONOLAB-CIT, temporal continuity of the electron density is incorporated to the reconstruction process by using Kalman filtering and smoothing techniques. As in previously proposed 3D-IONOLAB-CIT, a parametric model of the electron density distribution is formulated so that model parameters serve as the state in Kalman filtering/smoothing. In this parametric model for the electron density distribution, IRI-Plas model served as the base model. Two linear perturbation surfaces, each of which defined by three parameters and six parameters in total, are used to perturb the default foF2 and hmF2 surfaces of the IRI-Plas model so that its output distribution provides a better fit to the available measurements. This technique can work for any midlatitude region extending at most 12 degrees in latitude and 25 degrees in longitude, where linear assumption for foF2 and hmF2 holds. Using these six perturbation surface parameters as the state of the system, a Kalman filtering approach and a Kalman smoothing approach based on Rauch-Tung-Striebel smoother are implemented. Obtained result showed that using Kalman filtering/smoothing methods increase the reliability of reconstructions, especially when few number of GPS receiver stations are used in the reconstructions. Computational advantage of using the predictions by using the state transition model is also investigated. It is observed that initiating the optimization search in the problem space from the predicted values of perturbation surface parameters provide a computational saving of about 16–20%. In conclusion, the proposed 4D-IONOLAB-CIT technique provide robust reconstructions of the electron density distribution that is compliant with the physical properties of the ionosphere and yielding a close fit to the available measurements. Furthermore, by exploiting the temporal continuity through Kalman filtering/smoothing techniques, it has been demonstrated that reliable reconstructions can be obtained in stormy days even only a sparse set of measurements are available.

Acknowledgments

TNPGN RINEX data set is made available to IONOLAB group for TUBITAK109E055 project at http://www.ionolab.org/. This data set can be accessed by the permission from TUBITAK and General Command of Mapping of Turkish Army (http://www.hgk.msb.gov.tr/). This study is supported by TUBITAK EEEAG 115E915 and Joint TUBITAK EEEAG 114E092 and AS CR 14/001 grants.

References

Andreeva, E.S., Galinov, A.V., Kunitsyn, V.E., Melnichenko, Yu.A., Tereshchenko, E.E., Filimonov, M.A., Chernyakov, S.M., 1990. Radiotomographic reconstruction of ionization dip in the plasma near the earth. JETP Lett. 52, 145–148.

Arikan, O., Arikan, F., Erol, C.B., 2007. 3-D computerized ionospheric tomography with random field priors. In: Taş, K., Tenreiro Machado, J., Baleanu, D. (Eds.), Mathematical Methods in Engineering. Springer, Netherlands, pp. 325–334.

Armijo, L., 1966. Minimization of functions having Lipschitz continuous first partial derivatives. Pacific J. Math. 16, 1–3. <http://projecteuclid.org/euclid.pjm/1102995080>.

Austen, J.R., Franke, S.J., Liu, C.H., 1988. Ionospheric imaging using computerized tomography. Radio Sci. 23, 299–307.

Bilitza, D., Altadill, D., Zhang, Y., Mertens, C., Truhlik, V., Richards, P., McKinnell, L.A., Reinisch, B., 2014. The international reference ionosphere 2012 – a model of international collaboration. J. Space Weather Space Clim. 4, A07.

Bust, G.S., Garner, T.W., Gaussiran, T.L., 2004. Ionospheric data assimilation three-dimensional (IDA3D): a global, multisensor, electron density specification algorithm. J. Geophys. Res.: Space Phys. 109, A11312.

Erturk, O., Arikan, O., Arikan, F., 2009. Tomographic reconstruction of the ionospheric electron density as a function of space and time. Adv. Space Res. 43, 1702–1710.

Foster, J.C., Buonsanto, M.J., Holt, J.M., Klobuchar, J.A., Fougere, P., Pakula, W., Raymund, T.D., Kunitsyn, V.E., Andreeva, E.S., Tereshchenko, E.D., Khudukon, B.Z., 1994. Russian-american tomography experiment. Int. J. Imaging Syst. Technol. 5, 148–159.

Gulyaeva, T., Arikan, F., Hernandez-Pajares, M., Stanislawska, I., 2013. GIM-TEC adaptive ionospheric weather assessment and forecast system. J. Atmos. Solar Terr. Phys. 102, 329–340.

Gulyaeva, T.L., Bilitza, D., 2012. Towards ISO standard Earth ionosphere and plasmasphere model. In: Larsen, R.J. (Ed.), New Developments in the Standard Model. NOVA Science Publishers, Inc, Hauppauge, New York, pp. 1–48.

Gulyaeva, T.L., Stanislawska, I., 2008. Derivation of a planetary ionospheric storm index. Ann. Geophys. 26, 2645–2648.

Howe, B.M., Runciman, K., Secan, J.A., 1998. Tomography of the ionosphere: four-dimensional simulations. Radio Sci. 33, 109–128.

Jin, S., Park, J.U., 2007. Gps ionospheric tomography: a comparison with the iri-2001 model over South Korea. Earth Planets Space 59, 287–292.

Kalman, R.E., 1960. A new approach to linear filtering and prediction problems. J. Basic Eng., 35–45

Ma, X.F., Maruyama, T., Ma, G., Takeda, T., 2005. Three-dimensional ionospheric tomography using observation data of GPS ground receivers and ionosonde by neural network. J. Geophys. Res.: Space Phys. 110, A05308.

Mitchell, C.N., Spencer, P.S.J., 2003. A three-dimensional time-dependent algorithm for ionospheric imaging using GPS. Ann. Geophys. 46, 687–696.

Nayir, H., Arikan, F., Arikan, O., Erol, C.B., 2007. Total electron content estimation with Reg-Est. J. Geophys. Res.: Space Phys. 112, A11313.

Nesterov, I., Kunitsyn, V., 2011. Gnss radio tomography of the ionosphere: the problem with essentially incomplete data. Adv. Space Res. 47, 1789–1803.

Pryse, S., Kersley, L., 1992. A preliminary experimental test of ionospheric tomography. J. Atmos. Terr. Phys. 54, 1007–1012.

Rauch, H.E., Striebel, C.T., Tung, F., 1965. Maximum likelihood estimates of linear dynamic systems. AIAA J. 3, 1445–1450.

Raymund, T.D., Austen, J.R., Franke, S.J., Liu, C.H., Klobuchar, J.A., Stalker, J., 1990. Application of computerized-tomography to the investigation of ionospheric structures. Radio Sci. 25, 771–789.

Rius, A., Ruffini, G., Cucurull, L., 1997. Improving the vertical resolution of ionospheric tomography with GPS occultations. Geophys. Res. Lett. 24, 2291–2294.

Sayin, I., Arikan, F., Akdogan, K.E., 2010. Optimum temporal update periods for regional ionosphere monitoring. Radio Sci. 45, RS6018.

Scherliess, L., Schunk, R.W., Sojka, J.J., Thompson, D.C., 2004. Development of a physics-based reduced state Kalman filter for the ionosphere. Radio Sci. 39, RS1S04.

Tuna, H., Arikan, O., Arikan, F., 2015. Regional model-based computerized ionospheric tomography using GPS measurements: IONOLAB-CIT. Radio Sci. 50, 1062–1075, 2015RS005744.

Tuna, H., Arikan, O., Arikan, F., Gulyaeva, T.L., Sezen, U., 2014. Online user-friendly slant total electron content computation from IRI-Plas: IRI-Plas-STEC. Space Weather 12, 64–75.

Wang, C., Hajj, G., Pi, X., Rosen, I.G., Wilson, B., 2004. Development of the global assimilative ionospheric model. Radio Sci., 39, RS1S06

Wen, D., Yuan, Y., Ou, J., Zhang, K., Liu, K., 2008. A hybrid reconstruction algorithm for three dimensional ionospheric tomography. IEEE Trans. Geosci. Remote Sens. 46, 1733–1739.